

Ultrahigh concentration of NV^- centers embedded in the CVD epi-diamond layer near the interface with an HPHT diamond substrate

Yuanjie Yang(杨元杰), Shengran Lin(林盛然), Jiaxin Zhao(赵嘉昕), Changfeng Weng(翁长风), Liren Lou(楼立人), Wei Zhu(祝巍), and Guangzhong Wang(王冠中)

Citation : Chin. Phys. B, 2025, 34 (**5**): 056102. DOI: 10.1088/1674-1056/adc7f5
http://cpb.iphy.ac.cn; http://iopscience.iop.org/cpb

What follows is a list of articles you may be interested in

Effect of copper/tungsten heterophase interface on radiation resistance: Insights from atomistic simulations

Wen Chen(陈文), Min Li(李敏), Bao-Qin Fu(付宝勤), Tun Chen(陈暾), Jie-Chao Cui(崔节超), and Qing Hou(侯氢)
Chin. Phys. B, 2025, 34 (**4**): 046108. DOI: 10.1088/1674-1056/adb40d

Atomic origin of minor alloying element effect on glass forming ability of metallic glass

Shan Zhang(张珊), Qingan Li(李庆安), Yong Yang(杨勇), and Pengfei Guan(管鹏飞)
Chin. Phys. B, 2025, 34 (**3**): 036105. DOI: 10.1088/1674-1056/ada756

Dendritic tip selection during solidification of alloys: Insights from phase-field simulations

Qingjie Zhang(张清杰), Hui Xing(邢辉), Lingjie Wang(王灵杰), and Wei Zhai(翟薇)
Chin. Phys. B, 2024, 33 (**9**): 096103. DOI: 10.1088/1674-1056/ad57ac

Visualizing extended defects at the atomic level in a $Bi_2Sr_2CaCu_2O_{8+\delta}$ superconducting wire

Kejun Hu(胡柯钧), Shuai Wang(王帅), Boyu Li(李泊玉), Ying Liu(刘影), Binghui Ge(葛炳辉), and Dongsheng Song(宋东升)
Chin. Phys. B, 2024, 33 (**9**): 096101. DOI: 10.1088/1674-1056/ad6ccd

FL-Online: An x-ray crystallographic web-server for atomic-scale structure analysis of biomolecule

Bintang Wang(王宾堂), Tongxin Niu(牛彤欣), Haifu Fan(范海福), and Wei Ding(丁玮)
Chin. Phys. B, 2024, 33 (**7**): 076104. DOI: 10.1088/1674-1056/ad47e5

Ultrahigh concentration of NV^- centers embedded in the CVD epi-diamond layer near the interface with an HPHT diamond substrate

Yuanjie Yang(杨元杰), Shengran Lin(林盛然), Jiaxin Zhao(赵嘉昕), Changfeng Weng(翁长风), Liren Lou(楼立人), Wei Zhu(祝巍)[†], and Guanzhong Wang(王冠中)[‡]

Department of Physics, University of Science and Technology of China, Hefei 230026, *China*

(Received 19 February 2025; revised manuscript received 24 March 2025; accepted manuscript online 2 April 2025)

The negatively charged nitrogen vacancy (NV^-) center ensemble in as-grown chemical vapor deposition (CVD) diamond is a promising candidate for quantum sensing due to its long coherence time and excellent optical properties. However, achieving a high concentration of NV^- centers in as-grown CVD diamond remains a critical challenge, which constrains the performance of NV^- based sensors. In this study, we observe that NV^- center formation efficiency is significantly enhanced during the initial growth phase, with a coherence time T_2^* of 1.1 μs. These findings demonstrate that high-concentration NV^- centers can be achieved in as-grown diamonds, greatly enhancing their utility in high-performance magnetometers and quantum sensing.

Keywords: interface, high concentration, nitrogen vacancy centers, chemical vapor deposition (CVD), diamond

PACS: 61.72.J–, 81.05.ug, 68.35.Ct, 71.55.–i

DOI: 10.1088/1674-1056/adc7f5 **CSTR:** 32038.14.CPB.adc7f5

1. Introduction

The negatively charged nitrogen-vacancy (NV^-) center in diamond has received significant attention over the past few decades as a solid-state qubit,[1,2] particularly due to its long spin coherence time at room temperature.[3] Additionally, the electronic spin state of the NV^- center can be optically initialized and read out, as well as coherently manipulated by a microwave (MW) field with high fidelity.[4] The NV^- center in diamond has emerged as a leading platform for quantum technologies, demonstrating significant promise in applications such as quantum information processing[5] and quantum sensing.[6] Building on foundational advancements, including nanoscale magnetic resonance imaging[7] and quantum algorithm implementations,[8] NV^--based systems have achieved rapid progress in scalability,[9] integration,[10] and real-world applicability.[11] Recent breakthroughs further underscore the transformative potential of NV^- ensembles, particularly in enabling high-resolution vectorial magnetic field imaging.[12] For NV^--based magnetometers, the concentration and coherence time of NV^- centers are crucial parameters that directly affect sensitivity. However, achieving a high concentration of NV^- centers while maintaining long coherence times remains a significant challenge.[13,14] Currently, high-energy electron/ion irradiation followed by annealing is the most common method for obtaining high-concentration NV^- ensembles.[15,16] However, the high density of defects generated during irradiation reduces the coherence time of NV^- centers, thereby limiting the sensitivity of the resulting magnetometer.[17] Alternatively, NV^- centers can be synthesized directly during chemical vapor deposition (CVD), which is an effective method for generating NV^- centers with long coherence times. This approach offers the advantage of precise control over the concentrations of paramagnetic impurities and dislocations, thereby enhancing the overall quality of the resulting NV^- centers. The primary challenge for sensors based on as-grown NV^- centers is achieving a high NV concentration while maintaining optimal coherence properties. Increasing the nitrogen content in the precursor is the usual method for boosting the NV^- center concentration in CVD diamond. However, it has been reported that the NV^- center concentration saturates at approximately 10 ppb when the nitrogen content exceeds 100 ppm, leading to the diamond becoming brownish and non-epitaxial growth.[18] To address this issue, further work is needed to obtain high-concentration NV^- centers with excellent coherence properties for magnetic sensing applications.

Recently, Hei *et al.*[13] reported that the concentration of NV^- centers in as-grown CVD diamond varies spatially along the growth direction, with a higher concentration found in the region near the interface with the high-pressure high-temperature (HPHT) diamond substrate. These findings suggest that it is possible to achieve a high concentration of NV^-

[†]Corresponding author. E-mail: zhuw@ustc.edu.cn

[‡]Corresponding author. E-mail: gzwang@ustc.edu.cn

© 2025 Chinese Physical Society and IOP Publishing Ltd. All rights, including for text and data mining, AI training, and similar technologies, are reserved.

centers in that region, which could potentially enhance delta doping technology in CVD diamond — a development of significant interest in precision magnetic field sensing.[19] However, to fully realize this potential, further studies are required to determine the detailed distribution and coherence properties of NV^- centers formed at different growth stages.

In this paper, we focus on realizing a high concentration of NV^- centers with a long inhomogeneous dephasing time in CVD diamond. Fluorescence images revealed that a high concentration of NV^- centers was achieved in the grown region up to approximately 150 μm away from the interface. The highest NV^- concentration was determined to be 8.8 ppb in a region about 64 μm away from the interface. A long inhomogeneous dephasing time of $\sim 1.13 \pm 0.18$ μs for NV^- centers in that region was measured using the Ramsey fringe technique. These results suggest that the region near the interface may serve as a promising ensemble of high concentration NV^- centers with comparatively long coherence times, making it an excellent candidate for NV^- based magnetic sensors.

2. Experimental details

HPHT diamond, with dimensions of 3.5 mm × 3.5 mm × 1.0 mm, was used as the substrate. The concentration of nitrogen was determined to be about dozens ppm using the electron paramagnetic resonance, while the concentration of NV centers is below 5 ppb. Before epitaxial growth, the substrate was immersed in a boiling acid mixture ($HClO_4$:H_2SO_4:HCl = 1 : 1 : 1) at 200 °C for 2 hours, then ultrasonically cleaned with acetone, isopropyl alcohol, and deionized water respectively. After cleaning, the substrate was placed inside the growth chamber. To remove surface defects induced by mechanical polishing, the substrate was pre-treated with H_2/O_2 plasma for 10 min.[20] Following this, the diamond film was homoepitaxially deposited using the MW plasma CVD method. The diamond film was grown with a substrate temperature of 900 °C, MW power of 5.0 kW, chamber pressure of 150 Torr, and a methane concentration of 4%. The MW power of 5 kW and moderate chamber pressure (150 Torr) were selected to stabilize plasma conditions, ensuring uniform temperature distribution across the substrate and improving overall film homogeneity. The lower methane concentration effectively suppresses the formation of undesirable secondary phases, while maintaining a steady diamond growth rate. Appropriate substrate temperature enhances nitrogen adatom mobility, promoting substitutional incorporation into the diamond lattice while preventing polycrystalline nucleation and graphitization. During growth, 10 ppm of N_2 was introduced as a nitrogen source to facilitate NV^- center formation. After 55 hours of growth, a 0.8 mm thick epitaxial layer was obtained. To characterize the properties of the NV^- centers at various positions along the growth direction, the sample was transected using a Nd:YAG laser to cut the cross-section parallel to the growth direction, as illustrated schematically in Fig. 1(a). The cross-section was then carefully polished for characterization.

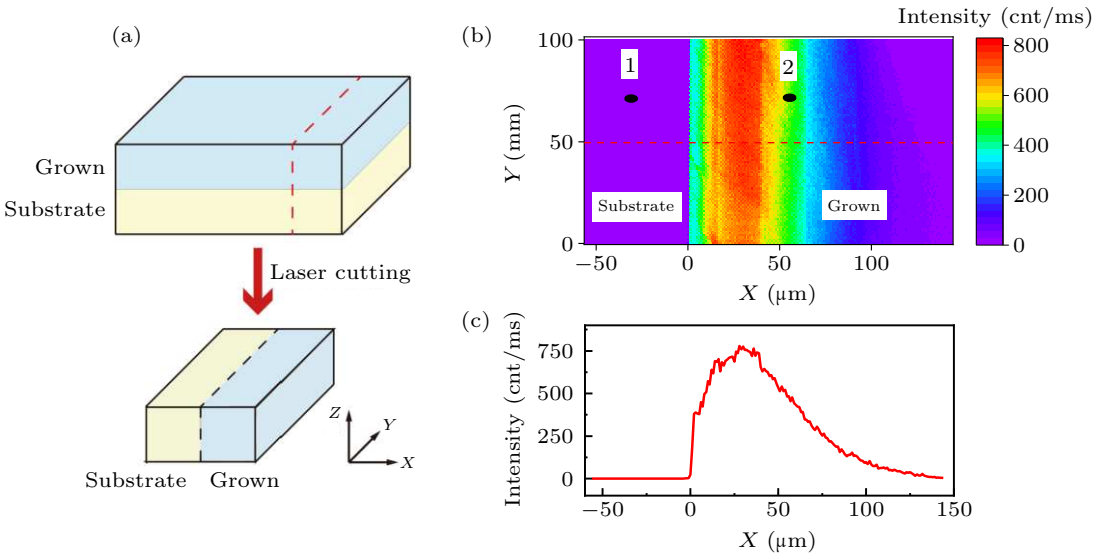


Fig. 1. (a) Schematic diagram of our sample: the yellow region represents the HPHT substrate, and the blue region represents the grown diamond epi-layer. The red dashed line in the upper part indicates the position of laser cutting. The coordinate axes shown in the lower part indicate the scanning direction of the CFM. (b) A fluorescence image obtained with a CFM, where the black points indicate the positions for spectral measurements. (c) Fluorescence scanning along the line across the interface, as marked in (b) with a red dashed line.

3. Results and discussion

To characterize the spatial distribution of NV^- centers in the epi-layer along the growth direction, the fluorescence image of the sample's cut-surface was measured using a home-built confocal microscope (CFM). A 532 nm green laser was used as excitation source, which was focused onto the diamond sample through an objective lens (Olympus, 100×, NA = 0.95). The resulting fluorescence was then collected

by the same objective and directed to avalanche photodiodes via a single-mode fiber. Only fluorescence with wavelengths from 600 nm to 800 nm was detected using a band-pass filter (BPF). The sample was carefully mounted on the CFM's sample platform with the growth direction of the epi-layer parallel to one of the platform's scanning directions (defined as the X axis), as shown in Fig. 1(a). Since the primary defect of type Ib HPHT diamond is neutral substitutional nitrogen (N_s^0), with few NV^- centers,[21] we attributed the bright fluorescence shown in Fig. 1(b) to the NV^- centers in the epi-layer. As illustrated in Fig. 1(b), the fluorescence intensity changed significantly along the epi-growth direction, reflecting the spatial variation of NV^- concentration in the grown diamond film.

Photoluminescence (PL) spectra were also measured by directing the collected fluorescence to a spectrometer (Jobin-Yvon HR800) via a single-mode fiber. Figure 2(a) shows the spatial distribution and charge states of the NV centers, revealing variations in luminescence characteristics across different regions of the sample. To minimize measurement errors arising from variations in testing conditions, we normalized the spectra using the first-order Raman peak in Fig. 2(b). Point 1 is located in the HPHT diamond substrate, and the corresponding spectrum showed no NV^- signal (neither the zero-phonon line (ZPL) at 637 nm nor the accompanying phonon sideband), consistent with previous reports.[22] Point 2 is located in the epi-layer near the interface, where the spectrum showed not only a sharper NV^- ZPL at 637 nm but also a significant peak at 737 nm, corresponding to the ZPL of the negatively charged silicon vacancy (SiV^-) center.

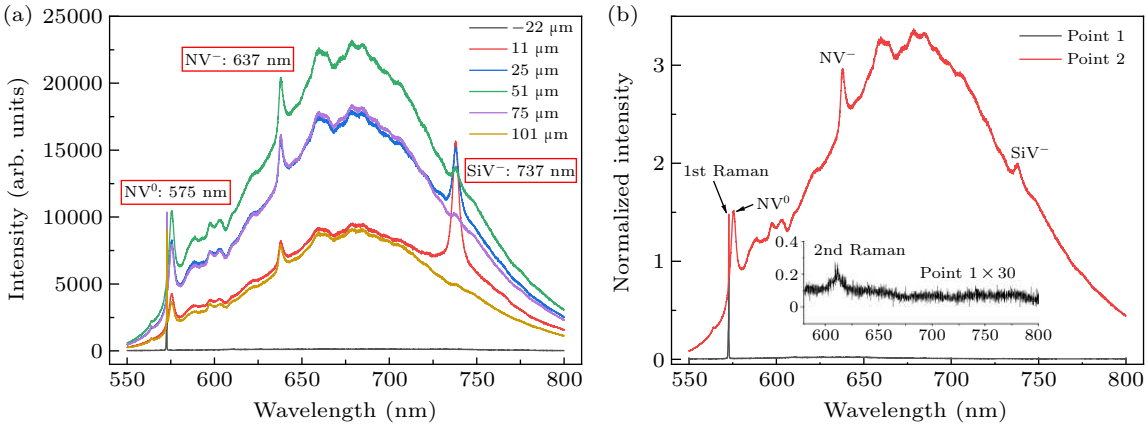


Fig. 2. (a) PL spectra at various key positions along the red dashed line in Fig. 1(b). The legend indicates the distance from the interface. (b) PL spectra at two typical positions, as indicated in Fig. 1(b). The black line represents the spectrum from the HPHT substrate, and the red line represents the spectrum from the epi-diamond in the region near the interface. The intensity is normalized with respect to the first-order Raman peak, and the inset shows the magnified signal from the area (30×).

Since the collected fluorescence originated from both NV^- centers and SiV^- centers, the fluorescence images in Figs. 1(b) and 1(c) do not accurately represent the distribution of NV^- centers in the epi-layer. To precisely characterize the distribution of NV^- and SiV^- centers along the growth direction, the integrated ZPL intensity distributions of the NV^- and SiV^- centers were derived from the recorded spectra and are shown in Fig. 3(c). Because the integrated ZPL intensity is proportional to the concentration of the corresponding color centers, the curves in Fig. 3(c) represent the relative concentration distributions of NV^- and SiV^- centers along the growth direction.

By comparing the integrated ZPL intensity of NV^- centers in our sample with that in a diamond of known NV^- concentration, we deduced the highest NV^- concentration to be approximately 1.5×10^{15} cm^{-3} (~ 8.8 ppb) in our sample. We estimated the NV^- center concentration of the standard sample by comparing its saturation luminescence intensity with that of single NV centers under the same system. Our sample corresponded to an NV^- doping efficiency of about 10^{-3} (the ratio of the concentration of NV^- centers to that of nitrogen in the gas sources). This efficiency is higher than the values of 10^{-4}–10^{-6}, previously reported for CVD-grown diamond.[23] Moreover, the concentration of NV^- centers is extremely high in the region within ~ 150 μm of the interface, with the highest concentration being about 50 times greater than that in the grown region far from the interface. This result suggests that NV^- centers are more easily generated during the initial growth stage of CVD diamond. Etch pits were observed on the HPHT diamond substrate after H_2/O_2 plasma treatment, as shown in Fig. 3(a). These etch pits are shaped like inverted pyramids, with exposed {111} facets. The etch pits expose underlying lattice defects, which serve as preferential nucleation sites for subsequent diamond growth. During growth, carbon atoms preferentially accumulate at defect sites, leading to the formation of growth hillocks.[13] It was previously reported that the {111} faces are 3–4 times more favorable for nitrogen atom incorporation than the {100} faces.[14] Thus, we suppose that the high NV^- center concentration observed in our sample is related to the pyramidal hillock growth during

the initial growth stage of CVD diamond.

However, the high nitrogen incorporation efficiency of the {111} face alone cannot fully explain the ultrahigh concentration of NV^- centers observed in our sample. Specifically, a 50-fold increase was observed in the concentration of NV^- centers in the epi-layer near the substrate compared to that in regions further away from the substrate. The activation energy for nitrogen atom diffusion in diamond is reported to be 5.0 ± 0.3 eV,[24] corresponding to a diffusion temperature significantly above the growth temperature of 900 °C. This indicates that the massive nitrogen atoms embedded in the HPHT diamond substrate contribute negligibly to the concentration of NV^- centers in the epi-layer. Furthermore, fluctuations in temperature and gas sources were slight during the growth process, minimizing their influence on NV^- center formation.

To investigate the cause of the high NV^- center concentration, we analyzed the variation in the concentration ratio of NV^- centers to neutral nitrogen vacancy (NV^0) centers in diamond (hereafter referred to as $[NV^-]/[NV^0]$) along the growth direction. As shown in the curves in Fig. 3(d), this ratio is lower near the interface. The NV^- center possesses an extra electron, with N_s^0 acting as the primary electron donor in our diamond sample. In diamonds with higher NV center formation efficiency (i.e., the ratio of NV center concentration to nitrogen concentration), a smaller proportion of nitrogen atoms remains available to act as electron donors, resulting in a lower $[NV^-]/[NV^0]$ ratio. Thus, the lower $[NV^-]/[NV^0]$ ratio near the interface suggests a high NV center formation efficiency in that region, which likely contributes to the high concentration of NV^- centers.

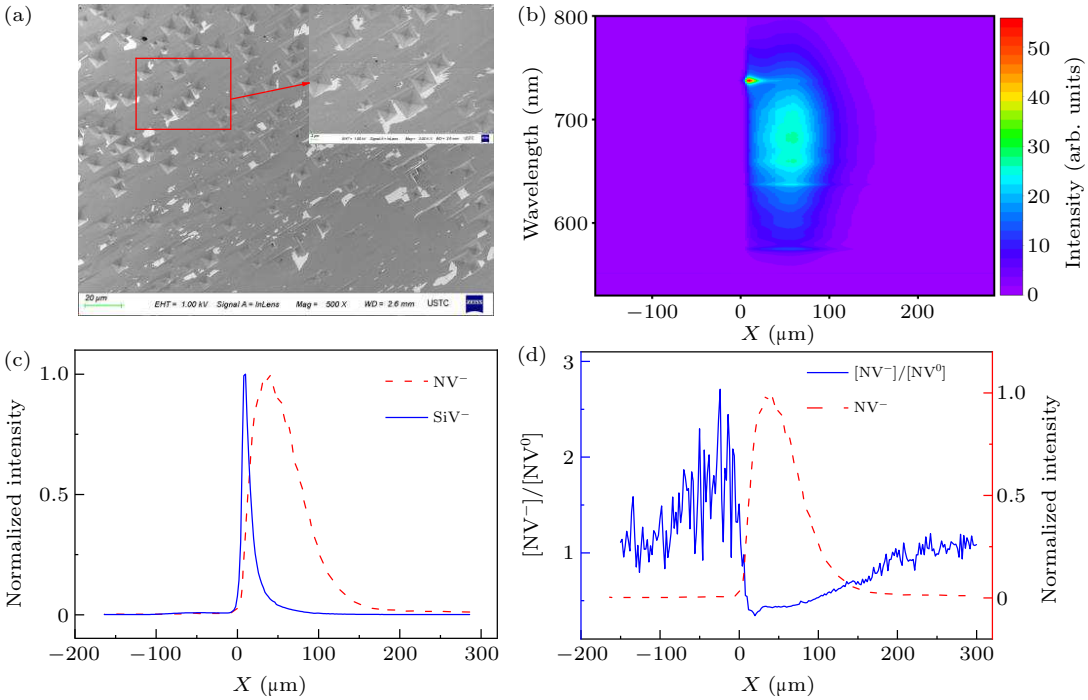


Fig. 3. (a) SEM image of the HPHT diamond substrate after H_2/O_2 plasma treatment. (b) Line mapping of PL intensity across the interface, with colors representing different PL intensities as indicated by the color bar. The intensity is normalized to the first-order Raman peak. (c) The relative distributions of the integrated ZPL intensities of NV^- centers (red) and SiV^- centers (blue) along the growth direction, with both lines normalized by dividing by their respective maximums. These lines also represent the relative concentration distribution of color centers. (d) The variation of the ratio $[NV^-]/[NV^0]$ along the growth direction. To conveniently identify the location relative to the interface, the curve for NV^- distribution (red line) is plotted on the same graph. The interface between the grown diamond and the HPHT substrate is located at approximately $X = 16$ μm. The severe oscillations in the curve at $X < 0$ μm are likely due to a few NV^- centers present in the HPHT diamond.

Additionally, Martineau *et al.*[25] reported that the dislocation density is higher near the substrate–epilayer interface compared to other regions. These dislocations act as preferential sites for vacancy aggregation, which promote vacancy stabilization. Consequently, it is presumed that vacancies are easier to form during the initial growth stage, facilitating NV^- center formation in proximity to the interface. It should be noted, however, that the region with the lowest $[NV^-]/[NV^0]$ ratio does not necessarily correspond to the highest NV^- concentration. This discrepancy may be due to variations in nitrogen at different growth stages or the formation of other nitrogen-related color centers, such as NVH^- and SiV^-.[26] These defects will capture a significant number of unpaired electrons from nitrogen, thereby reducing the availability of free electrons for the formation of NV^- centers and consequently decreasing the ratio of $[NV^-]/[NV^0]$.

For the SiV^- center, a narrower distribution was observed in the diamond sample [see Fig. 3(c)]. Since no silicon was introduced through the gas source, we inferred that the silicon atoms were introduced during the H_2/O_2 plasma etching

of the quartz window. As shown in Fig. 2(a), the fluorescence from the SiV^- centers partially overlaps with that of the NV^- centers and cannot be filtered out using the BPF designed to isolate fluorescence solely from the NV^- centers. To eliminate the influence of the SiV^- centers, we proposed minimizing the residual Si in the chamber through a CH_4/H_2 flushing process (with no MW applied) inserted after the H_2/O_2 plasma treatment.[27]

Optically detected magnetic resonance (ODMR) measurements were also performed to determine the inhomogeneous dephasing times T_2^* of the NV^- centers in the sample. To manipulate the electron spin state of the NV^- center, a static magnetic field of 21.4 Gauss was applied to lift the $|m_s = \pm 1\rangle$ spin sublevels, and an MW field was applied using a copper wire with a diameter of 20 μm stretched across the diamond sample. Figure 4(a) presents the continuous-wave (CW) ODMR spectrum, showing four pairs of resonances corresponding to the NV^- centers oriented along the four different $\langle 111 \rangle$ axes. The resonance peaks exhibit power broadening effects.[28] By properly adjusting the MW and laser power, we obtained a refined CW ODMR spectrum around 2810 MHz, as shown in the inset of Fig. 4(a). The observed peak splitting was due to the hyperfine interaction with the nuclear spin of ^{14}N. Next, we applied a Ramsey MW pulse sequence, $\pi/2 \sim \tau \sim \pi/2$, to determine the T_2^*. Figure 4(b) showed the recorded Ramsey fringe. Due to the interaction with ^{14}N nuclear spin, the oscillation consists of three frequency components, $\Delta - 2.2$ MHz, Δ, and $\Delta + 2.2$ MHz, where Δ is the MW detuning from the central peak in the inset of Fig. 4(a). By fitting the Ramsey fringe with a function of $\exp[-(t/T_2^*)^2]\sum_{i=1}^{3}\cos(2\pi\sigma_i t + \phi_i)$,[29] we deduced an inhomogeneous dephasing time of $T_2^* \approx 1.13 \pm 0.18$ μs, which closely matches the value obtained from the single NV^- center in diamond with ^{13}C of natural abundance ($[^{13}C] = 1.1\%$).[30] This value is relatively high among the reported values,[23] which is primarily attributed to the high NV center formation efficiency, as well as low density of growth defects. The presence of paramagnetic defects during the growth process can adversely affect the coherence time of the NV^- centers. By enhancing MW power density and reducing the methane concentration,[31] we have achieved a diamond with a low defect density. Furthermore, figure 4(c) shows that T_2^* varied little along the epi-layer at various positions, indicating that nitrogen in the diamond contributed minimally to dephasing. As reported by Acosta *et al.*,[32] the interaction with ^{13}C nuclear spins is another cause of dephasing. It can be inferred that ^{13}C nuclear spins are the main dephasing source in our sample. To further prolong the dephasing time of NV^- center, the use of isotope purification technology is necessary. By utilizing purified isotope ^{12}C, Kleinssser *et al.* obtained a T_2^* of ~ 1.5 μs in diamond with an NV^- center concentration of ~ 1 ppm.[33] To demonstrate DC magnetic sensing based on the Ramsey fringes method, we recorded the Ramsey fringes before and after the magnetic field changed. As shown in Fig. 4(d),

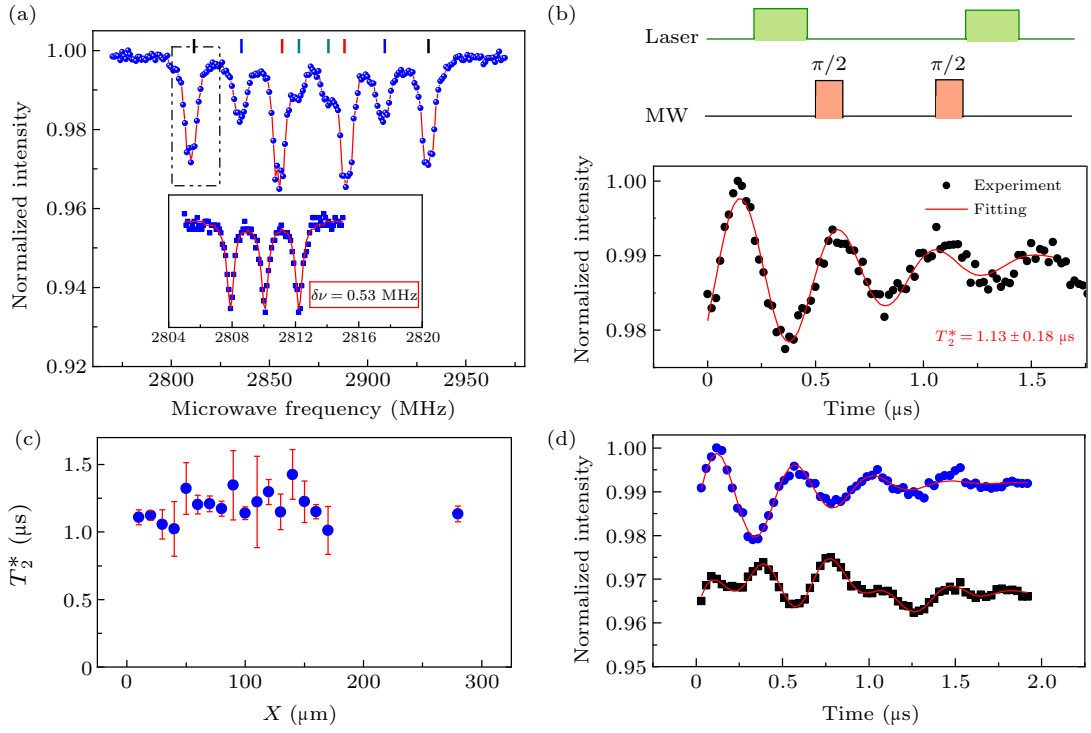


Fig. 4. (a) CW ODMR spectrum. The peaks are fitted using a Lorentzian function. The inset shows the hyperfine splitting of the resonant peak located at 2810 MHz, determined using ultralow MW power. The three peaks, with FWHM = 0.53 MHz, are attributed to the interaction with the ^{14}N nuclear spin. (b) Ramsey fringe. The upper is the corresponding measurement sequence. (c) The distribution of T_2^* along the growth direction. $X = 0$ indicates the interface. (d) Ramsey fringes under different applied magnetic fields. The Ramsey fringe at a lower magnetic field is compared to that at a slightly higher magnetic field.

the recorded Ramsey fringes show different oscillation, and the detuning Δ values were determined to be 0.008 MHz and 0.651 MHz, respectively, indicating a difference in magnetic field to be 1.800 Gauss. As demonstrated in Ref. [34], the minimum detectable DC magnetic field of an NV^- ensemble is

$$\delta B \cong \frac{\hbar}{g_s \mu_B} \frac{1}{R\sqrt{\eta}} \frac{1}{\sqrt{ntT_2^*}}, \tag{1}$$

where $g_s = 2.0028$ is the g-factor of NV^- center, μ_B is the Bohr magneton, R is the measurement contrast, η is the detection efficiency, n is the number of NV^- centers involved in the measurement, and t is the integration time. According to Eq. (1), we estimated the sensitivity of our sample to be 13.3 nT·Hz$^{-1/2}$. The sensitivity can be further improved by utilizing side-collection technology[35] and isotope purification technology. Additionally, increasing the concentration of NV^- center in the epi-layer near the interface is also advantageous.

4. Summary

In summary, we investigated the concentration and coherence properties of NV^- centers formed during the initial growth stage. Our results indicate that a narrow region near the interface between the substrate and the epitaxial diamond layer exhibits both a substantially higher NV^- center concentration and an extended inhomogeneous dephasing time compared to other areas. We anticipate that the concentration of NV^- centers can be further increased by optimizing the growth conditions, such as adjusting the substrate temperature, using N_2O as a dopant gas[23] and introducing a CH_4/H_2 flushing step following the H_2/O_2 etching. Moreover, our findings reveal that the NV^- center concentration peaks approximately 64 μm from the substrate in our experiment. This provides valuable insight that optimizing the timing of nitrogen dopant gas introduction in delta-doped diamond can lead to higher NV^- incorporation. Integrating these strategies with our growth technique can establish optimal conditions for achieving a high NV^- center concentration with minimal defects, thereby enhancing the application potential of diamond NV center in quantum sensing.

Acknowledgment

Project supported by the National Natural Science Foundation of China (Grant Nos. 11374280 and 50772110).

References

[1] Takeuchi M, Yasuoka M, Ishii M, Ohtani N and Shikata S 2023 *Diam. Relat. Mater.* **140** 110510
[2] Zou D, Shen S, Li L, Wang Q, Liang K, Chen L, Wu G and Shen W 2024 *Phys. B* **676** 415614
[3] Bai R, Zhu X, Yang F, Gao T, Wang Z, Yu L, Wang J, Zhou L and Du G 2022 *Chin. Phys. B* **31** 074203
[4] Wang J, Feng F, Zhang J, Chen J, Zheng Z, Guo L, Zhang W, Song X, Guo G, Fan L, Zou C, Lou L, Zhu W and Wang G 2015 *Phys. Rev. B* **91** 155404
[5] Xu K, Xie T, Li Z, Xu X, Wang M, Ye X, Kong F, Geng J, Duan C, Shi F and Du J 2017 *Phys. Rev. Lett.* **118** 130504
[6] Masuyama Y, Suzuki K, Hekizono A, Iwanami M, Hatano M, Iwasaki T and Ohshima T 2021 *Sensors* **21** 977
[7] Budakian R, Finkler A, Eichler A, Poggio M, Degen C L, Tabatabaei S, Lee I, Hammel P C, Eugene S P, Taminiau T H, Walsworth R L, London P, Bleszynski Jayich A, Ajoy A, Pillai A, Wrachtrup J, Jelezko F, Bae Y, Heinrich A J, Ast C R, Bertet P, Cappellaro P, Bonato C, Altmann Y and Gauger E 2024 *Nanotechnology* **35** 412001
[8] Atatüre M, Englund D, Vamivakas N, Lee S Y and Wrachtrup J 2018 *Nat. Rev. Mater.* **3** 38
[9] Delle Donne C, Iuliano M, Van Der Vecht B, Ferreira G M, Jirovská H, Van Der Steenhoven T J W, Dahlberg A, Skrzypczyk M, Fioretto D, Teller M, Filippov P, Montblanch A R P, Fischer J, Van Ommen H B, Demetriou N, Leichtle D, Music L, Ollivier H, Te Raa I, Kozlowski W, Taminiau T H, Pawełczak P, Northup T E, Hanson R and Wehner S 2025 *Nature* **639** 321
[10] Shandilya P K, Flagan S, Carvalho N C, Zohari E, Kavatamane V K, Losby J E and Barclay P E 2022 *J. Light. Technol.* **40** 7538
[11] Basu T, Patra A, Murali M, Saini M, Banerjee A and Som 2025 *ACS Omega* **10** 2372
[12] Liu X, Cui J, Sun F, Song X, Feng F, Wang J, Zhu W, Lou L and Wang G 2013 *Appl. Phys. Lett.* **103** 143105
[13] Hei L F, Zhao Y, Wei J J, Liu J L, Li C M, Tang W Z and Lu F X 2016 *Diam. Relat. Mater.* **69** 33
[14] Samlenski R, Haug C, Brenn R, Wild C, Locher R and Koidl P 1995 *Appl. Phys. Lett.* **67** 2798
[15] Feng F, Wang J, Zhang W, Zhang J, Lou L, Zhu W and Wang G 2016 *Appl. Phys. A* **122** 944
[16] Yokota Y, Kawarada H and Hiraki A 1990 *Jpn. J. Appl. Phys.* **29** L2232
[17] Romach Y, Müller C, Unden T, Rogers L J, Isoda T, Itoh K M, Markham M, Stacey A, Meijer J, Pezzagna S, Naydenov B, McGuinness L P, Bar-Gill N and Jelezko F 2015 *Phys. Rev. Lett.* **114** 017601
[18] Hounsome L S, Jones R, Martineau P M, Fisher D, Shaw M J, Briddon P R and Öberg S 2006 *Phys. Rev. B* **73** 125203
[19] Ohno K, Joseph Heremans F, Bassett L C, Myers B A, Toyli D M, Bleszynski Jayich A C, Palmstrøm C J and Awschalom D D 2012 *Appl. Phys. Lett.* **101** 082413
[20] Tallaire A, Achard J, Silva F, Sussmann R S, Gicquel A and Rzepka E 2004 *Phys. Status Solidi A* **201** 2419
[21] Woods G S, Van Wyk J A and Collins A T 1990 *Philos. Mag. B* **62** 589
[22] Liu J L, Zheng Y T, Lin L Z, Zhao Y, Chen L X, Wei J J, Wang J J, Guo J C, Feng Z H and Li C M 2018 *J. Mater. Sci.* **53** 13030
[23] Tallaire A, Mayer L, Brinza O, Pinault-Thaury M A, Debuisschert T and Achard J 2017 *Appl. Phys. Lett.* **111** 143101
[24] Anon
[25] Martineau P M, Lawson S C, Taylor A J, Quinn S J, Evans D J F and Crowder M J 2004 *Gems Gemol.* **40** 2
[26] Edmonds A M, D'Haenens-Johansson U F S, Cruddace R J, Newton M E, Fu K M C, Santori C, Beausoleil R G, Twitchen D J and Markham M L 2012 *Phys. Rev. B* **86** 035201
[27] Bou P, Vandenbulcke L, Herbin R and Hillion F 1992 *J. Mater. Res.* **7** 2151
[28] Dréau A, Lesik M, Rondin L, Spinicelli P, Arcizet O, Roch J F and Jacques V 2011 *Phys. Rev. B* **84** 195204
[29] Hu X, Liu G Q, Xu Z C and Pan X Y 2012 *Chin. Phys. Lett.* **29** 024210
[30] Dutt M V G, Childress L, Jiang L, Togan E, Maze J, Jelezko F, Zibrov A S, Hemmer P R and Lukin M D 2007 *Science* **316** 1312
[31] Ding S, Zhang J, Su K, Ren Z, Chen J, Yang Z, Zhang J and Hao Y 2024 *Sci. China Mater.* **67** 2329
[32] Acosta V M, Bauch E, Ledbetter M P, Santori C, Fu K M C, Barclay P E, Beausoleil R G, Linget H, Roch J F, Treussart F, Chemerisov S, Gawlik W and Budker D 2009 *Phys. Rev. B* **80** 115202
[33] Kleinsasser E E, Stanfield M M, Banks J K Q, Zhu Z, Li W D, Acosta V M, Watanabe H, Itoh K M and Fu K M C 2016 *Appl. Phys. Lett.* **108** 202401
[34] Maertz B J, Wijnheijmer A P, Fuchs G D, Nowakowski M E and Awschalom D D 2010 *Appl. Phys. Lett.* **96** 092504
[35] Le Sage D, Pham L M, Bar-Gill N, Belthangady C, Lukin M D, Yacoby A and Walsworth R L 2012 *Phys. Rev. B* **85** 121202